Ilam University of Medical Sciences

Plant Biotechnology Persa

Online ISSN: 2676-7414

Homepage: https://pbp.medilam.ac.ir

Development and Optimization of Three-Dimensionally Printed Polylactic Acid/Titanium Dioxide Scaffolds Incorporating Curcumin for Bone Tissue Engineering and Regeneration

Mozhgan Bagheri Doulabifard[1], Nahid Hassanzadeh Nemati [2]✉, Ahmad Ramezani Saadatabadi[3]

[1]Department of Biomedical Engineering, SR.C., Islamic Azad University, Tehran, Iran
[2]Department of Biomedical Engineering, SR.C., Islamic Azad University, Tehran, Iran
[3]Department of Chemistry, Sharif University, Tehran, Iran

Article Info

Article type:
Original Article

Article History:
Received: 10 Jun 2025
Revised: 18 Sep 2025
Accepted: 21 Jan 2025
Published Online: 20 Apr 2026

✉ ***Correspondence to:***
Nahid Hassanzadeh Nemati

Email:
nahid_hassanzadeh@iau.ac.ir

A B S T R A C T

Objective: *Curcuma longa L. (turmeric) is a medicinal plant rich in bioactive compounds, particularly curcumin, which exhibits antioxidant, anti-inflammatory, antimicrobial, and osteogenic properties. However, its poor aqueous solubility and limited bioavailability restrict its biomedical applications. Therefore, localized and controlled delivery systems may improve the therapeutic potential of curcumin for bone tissue regeneration.*

Methods: In the present study, turmeric-derived curcumin was incorporated as a plant-based bioactive compound into three-dimensionally printed polylactic acid/titanium dioxide (PLA/TiO_2) scaffolds designed for bone tissue engineering. Two curcumin-loading strategies were investigated and compared: (i) direct incorporation of curcumin into the printing ink (PTC) and (ii) post-printing coating of PLA/TiO_2 scaffolds with a hydroxypropyl methylcellulose–curcumin layer (PT/HC).

Results: Both scaffold types successfully incorporated curcumin while maintaining their porous structure. FTIR confirmed curcumin incorporation without significant changes in the matrix. PT/HC showed slightly higher swelling and a two-stage degradation profile. Both scaffolds exhibited favorable cellular responses, with cell viability above 85%; however, PTC showed significantly higher viability than PT/HC.

Conclusion: Overall, curcumin incorporation into PLA/TiO_2 scaffolds showed promise for bone tissue engineering. Direct incorporation provided superior biological performance while maintaining scaffold stability and cellular compatibility, supporting its potential as a localized delivery strategy for bone regeneration.

Keywords: Curcumin, *Curcuma longa*, Tissue Scaffolds, Bone Regeneration, Printing, Three-Dimensional, Titanium Dioxide

➢ **How to cite this paper**
Bagheri Doulabifard M, Hassanzadeh Nemati N, Ramezani Saadatabadi A. Development and Optimization of Three-Dimensionally Printed Polylactic Acid/Titanium Dioxide Scaffolds Incorporating Curcumin for Bone Tissue Engineering and Regeneration. Plant Biotechnology Persa. 2026; 8(3): Proof.

Introduction

Bone is one of the most important connective tissues in the human body, providing structural support and maintaining skeletal integrity while protecting and supporting vital organs. It also serves as the principal reservoir of minerals, particularly calcium and phosphorus, and consequently plays a central role in mineral homeostasis. In addition, bone marrow is the primary site of hematopoiesis [1,2]. Despite its intrinsic regenerative capacity, bone tissue can undergo extensive damage or loss as a result of trauma, disease, infection, congenital abnormalities, and other pathological conditions

DOI: 10.61882

Publisher: Ilam University of Medical Sciences

attractive candidates for the development of bioactive biomaterials designed to support tissue repair and regeneration. Among medicinal plants, *Curcuma longa* L. (family Zingiberaceae), commonly known as turmeric, is particularly noteworthy because of its long history of medicinal use and its abundance of biologically active constituents. The rhizome of *C. longa* contains a group of polyphenolic compounds collectively known as curcuminoids, among which curcumin is the best characterized and most extensively investigated constituent in pharmacological and biomedical research. *Curcuma longa* L. (turmeric), as a medicinal plant rich in bioactive compounds, particularly curcumin, provides an important link between medicinal-plant research and modern biotechnology in tissue engineering. With antioxidant, anti-inflammatory, and antimicrobial properties, curcumin represents a promising plant-derived bioactive component for enhancing the biological functionality of engineered scaffolds. Curcumin, a major bioactive constituent of *C. longa*, exhibits a broad spectrum of biological activities, including antioxidant, anti-inflammatory, antimicrobial, and cell-regulatory effects [17,18]. These properties are particularly relevant to bone regeneration because excessive inflammation, oxidative stress, and microbial infection can disrupt the tightly regulated cellular and molecular processes required for effective bone healing. Previous studies have suggested that curcumin may influence osteogenic processes and bone regeneration through modulation of inflammatory and oxidative-stress pathways and through effects on the proliferation, adhesion, and differentiation of bone-related cells [17,18]. Accordingly, turmeric-derived curcumin represents a promising plant-derived bioactive compound for incorporation into tissue-engineered scaffolds and other regenerative biomaterial systems.

Despite its considerable biological potential, the direct application of curcumin remains challenging because of its poor aqueous solubility, limited stability, and low systemic bioavailability, which can restrict its effective delivery and biological availability at the target site. The development of localized and controlled-delivery systems may therefore provide an effective approach for improving the local availability of curcumin while minimizing limitations associated

[3]. The progressive aging of the global population has further intensified this clinical challenge, as aging is associated with an increased incidence of skeletal disorders and a reduced capacity for effective bone repair [4,5].

Current clinical strategies for the treatment of substantial bone defects, including autologous and xenogeneic bone grafting, are associated with several limitations. These include the risk of infectious disease transmission, limited availability of suitable graft material, donor-site morbidity, the need for additional surgical procedures, and complications associated with tissue harvesting [6]. These limitations have stimulated the development of alternative approaches that are biocompatible, structurally appropriate, and capable of supporting the complex biological processes involved in bone repair. Among the strategies receiving increasing attention is the use of three-dimensionally (3D) printed scaffolds for tissue engineering and the treatment of bone defects [7,8].

In 3D-printing-based tissue engineering, biomaterial formulations or bioinks are deposited layer by layer according to a predefined digital design to produce three-dimensional scaffolds with controlled architectures [9,10]. This technology has expanded the possibilities for scaffold fabrication by enabling precise control over geometry and pore architecture, facilitating patient-specific designs, and, in selected applications, allowing cells or bioactive agents to be incorporated during fabrication [11,12]. Such versatility is particularly advantageous in bone tissue engineering, where scaffold architecture, porosity, mechanical integrity, degradation behavior, and biological functionality must be carefully coordinated. Accordingly, 3D printing was selected in the present study as the fabrication approach for producing the engineered scaffolds.

In parallel with advances in scaffold-based tissue engineering, increasing attention has been directed toward medicinal plants and plant-derived bioactive compounds as potential components of innovative tissue-regenerative strategies. Medicinal plants are rich sources of secondary metabolites with diverse biological activities, including antioxidant, anti-inflammatory, antimicrobial, and cell-regulatory effects. These properties make plant-derived compounds

represent two fundamentally different modes of incorporating the plant-derived bioactive compound: incorporation within the bulk scaffold matrix during fabrication versus post-fabrication surface loading.

Despite substantial progress in the development of 3D-printed scaffolds for bone tissue engineering, limited information is available regarding the influence of different loading strategies for plant-derived bioactive compounds, particularly curcumin, on the physicochemical and biological performance of PLA/TiO_2-based scaffolds. Direct comparison of curcumin incorporated during the printing process with curcumin deposited as a polymeric surface coating after printing may therefore provide valuable insight into the suitability of different incorporation strategies for localized delivery of this plant-derived compound while preserving the structural and biological properties of the scaffold.

Accordingly, the present study aimed to fabricate 3D-printed PLA/TiO_2 scaffolds incorporating turmeric-derived curcumin using two different loading strategies direct incorporation of curcumin into the printing formulation and post-printing surface coating with an HPMC-based curcumin formulation and to compare their physicochemical and biological performance.

Despite numerous studies on curcumin and 3D-printed scaffolds, a direct comparison of curcumin incorporation into the PLA/TiO_2 matrix before printing versus post-printing surface coating has not been sufficiently investigated. This gap is important because the loading strategy may influence curcumin distribution and availability, scaffold properties, and cellular responses. Therefore, the present study addresses this gap by directly comparing these two loading strategies. The effects of the curcumin-loading strategy on scaffold morphology, chemical composition, swelling behavior, biodegradation, cellular morphology, and cell viability were subsequently evaluated. The ultimate objective was to identify a suitable approach for incorporating and locally delivering curcumin within a bioactive scaffold platform with potential applications in bone tissue engineering and regeneration.

Materials and Methods

Materials

with conventional administration. Integrating a bioactive compound derived from a medicinal plant with a tissue-engineered scaffold offers a potentially complementary strategy that combines the biological properties of the phytochemical with the structural and functional advantages of biomaterials.

The composition of the printing formulation is another important determinant of the physicochemical and biological properties of the resulting scaffold [13]. In the present study, polylactic acid (PLA) was selected as the principal scaffold-forming polymer because of its biodegradability, biocompatibility, favorable mechanical properties, and established use in tissue-engineering applications [14,15]. However, the intrinsic biological functionality of PLA is relatively limited. Titanium dioxide (TiO_2) was therefore incorporated into the PLA matrix to modify the functional properties of the composite scaffold. In addition to influencing the physicochemical characteristics of the material, TiO_2 has been reported to exhibit antimicrobial properties, which may be advantageous for biomaterials intended for bone repair and regeneration [16].

Combining a plant-derived bioactive compound such as curcumin with a PLA/TiO_2 scaffold may provide complementary advantages. The three-dimensional scaffold can serve as a localized platform for retaining and delivering curcumin at the site of bone injury, while the biological activities of curcumin may enhance the bioactive functionality of the scaffold and potentially contribute to a more favorable microenvironment for cellular processes associated with tissue repair. However, the method used to incorporate curcumin into the scaffold can substantially influence its distribution, availability, release characteristics, physicochemical properties, and cellular response.

In the present study, curcumin was incorporated into the scaffolds using two distinct loading strategies. In the first approach, curcumin was directly incorporated into the PLA/TiO_2 printing formulation before 3D printing. In the second approach, curcumin was incorporated after scaffold fabrication by applying a hydroxypropyl methylcellulose (HPMC)-based surface coating to preformed PLA/TiO_2 scaffolds. These approaches

optimized printing parameters established for the designed scaffold architecture.

Preparation of the Hydroxypropyl Methylcellulose/Curcumin Coating

To prepare the HPMC/curcumin coating formulation, an HPMC solution was first prepared at a concentration of 2% (w/v). Briefly, 2 g of HPMC powder was gradually added to 100 mL of preheated deionized water maintained at 50–60 °C under continuous stirring. This gradual addition was performed to minimize polymer agglomeration and facilitate uniform hydration and dissolution. The mixture was magnetically stirred for 2–3 h at the same temperature range until a homogeneous HPMC solution was obtained.

In parallel, curcumin was dissolved in 75% ethanol at a concentration equivalent to 2% (w/w) relative to the HPMC content. The curcumin solution was maintained at 40–50 °C under continuous stirring until complete dissolution was achieved. The curcumin solution was then added dropwise to the HPMC solution, and the resulting mixture was stirred for an additional 1–2 h at 40–50 °C to ensure uniform incorporation of curcumin into the polymeric phase.

Citric acid was subsequently added at 15% (w/w) relative to HPMC as a cross-linking agent, and the formulation was stirred for a further 30 min to obtain the final coating solution.

Prior to coating, the surfaces of the PLA/TiO_2 scaffolds were activated to improve surface wettability and promote coating adhesion. The scaffolds were first immersed in 70% ethanol for 15 min and subsequently in deionized water for 15 min. The samples were then treated with 0.5 M sodium hydroxide solution for 30 min to increase the availability of polar functional groups on the scaffold surface. After thorough washing, the activated PLA/TiO_2 scaffolds were immersed in the HPMC/curcumin formulation and coated by a dip-coating procedure.

Following immersion, the scaffolds were carefully withdrawn from the coating solution to allow excess formulation to drain from their surfaces. The coated samples were subsequently placed in an oven at 120 °C for approximately 15 min to facilitate coating stabilization and cross-linking.

Polylactic acid (PLA) was purchased from NatureWorks (USA) with a melt flow rate of 6 g/10 min. Titanium dioxide (TiO_2) nanoparticles were supplied by Nanoavaran Nanoscale Borhan (Iran), hydroxypropyl methylcellulose (HPMC) was obtained from Temad Kala (Iran), and curcumin was supplied by Exir Nano Sina (Iran). Chloroform, citric acid, and sodium hydroxide were purchased from Merck (Germany), whereas ethanol, dimethyl sulfoxide (DMSO; 1X), and thiazolyl blue tetrazolium bromide (MTT) were obtained from Sigma-Aldrich (USA).

For the biological assays and cell culture experiments, cell culture medium, fetal bovine serum (FBS), and penicillin–streptomycin antibiotic solution was obtained from Gibco (Life Technologies, USA). Phosphate-buffered saline (PBS) was purchased from Temad Kala (Iran). The L929 cell line was obtained from the Cell Bank of the Pasteur Institute of Iran (National Cell Bank of Iran, Tehran) and used for the subsequent cellular assays.

Preparation of Printing Inks and Three-Dimensional Printing

A predefined porous scaffold architecture suitable for bone tissue engineering was initially designed using SOLIDWORKS software. Following completion of the digital design, the printing formulations required for three-dimensional scaffold fabrication were prepared. PLA was dissolved in chloroform at a concentration of 17% (w/v), and the resulting solution was magnetically stirred at room temperature for 1 h to ensure complete dissolution of the polymer. TiO_2 nanoparticles were then incorporated at a concentration corresponding to 3% (w/w) relative to the polymer. The suspension was magnetically stirred for 1 h and subsequently subjected to ultrasonication for 30 min to promote homogeneous nanoparticle dispersion throughout the polymer matrix.

For the curcumin-containing formulation, curcumin powder was added at 2% (w/w) and the mixture was continuously stirred for 4 h to obtain a uniform printing ink. The prepared formulations were subsequently transferred into syringes and loaded into a CSS1 three-dimensional printer (Chekad Sanat Espadan, Iran). Scaffold fabrication was then performed according to the

composition and coding of the fabricated scaffold groups are presented in Table 1.

Finally, the scaffolds were rinsed with deionized water and dried under appropriate conditions. The

Table 1: Composition and coding of the fabricated scaffolds

No.	Scaffold code	Base composition	Surface coating
1	PT	Polylactic acid/titanium dioxide (PLA/TiO_2)	None
2	PTC	Polylactic acid/titanium dioxide/curcumin (PLA/TiO_2/curcumin)	None
3	PT/HC	Polylactic acid/titanium dioxide (PLA/TiO_2)	Hydroxypropyl methylcellulose containing curcumin (HPMC/curcumin)

of 10–80° at a voltage of 40 kV and a current of 30 mA at room temperature. The resulting diffraction patterns were used to evaluate structural changes and identify the crystalline phases present in the fabricated scaffolds.

Swelling Behavior

The water-uptake capacity of the scaffolds was evaluated by determining their swelling ratio in phosphate-buffered saline (PBS). Briefly, the initial dry weight of each scaffold (W_0) was recorded. The samples were then immersed in 30 mL of PBS and incubated for 24 h in a thermoshaker maintained at 37 ± 0.5 °C. After incubation, the scaffolds were removed from the solution, and excess surface moisture was gently blotted away. The swollen weight (W_1) was subsequently measured. The swelling percentage of each scaffold was calculated using Equation [19]:

$$\text{Swelling (\%)} = [(W_1 - W_0) / W_0] \times 100$$

Biodegradation Assessment

The degradation behavior of the scaffolds under simulated physiological conditions was evaluated by measuring their percentage weight loss following incubation in phosphate-buffered saline (PBS). Briefly, the initial dry weight of each scaffold (W_1) was recorded before incubation. The scaffolds were then immersed individually in 30

Scaffold Characterization

To evaluate the structural characteristics and surface morphology of the fabricated scaffolds, macroscopic images of the samples were first acquired using a 5-megapixel digital camera. The scaffold microstructure, uniformity of the printed filaments, pore dimensions and distribution, and surface morphology were subsequently examined by field-emission scanning electron microscopy (FE-SEM; Vega3, TESCAN, Czech Republic). Prior to imaging, the samples were sputter-coated with a thin layer of gold to improve surface conductivity and enhance image quality.

Fourier-transform infrared spectroscopy (FTIR) was performed to identify the functional groups present in the scaffolds and to assess chemical changes associated with the incorporation of titanium dioxide, curcumin, and the HPMC coating. For this analysis, the samples were ground into a fine powder and mixed with 100 mg of potassium bromide (KBr). FTIR spectra were then recorded using a Thermo Nicolet Avatar spectrometer over the wavenumber range of 400–4000 cm^{-1} and subsequently analyzed to identify the characteristic absorption bands of the scaffold constituents.

The crystalline structure and constituent phases of the scaffolds were characterized by X-ray diffraction (XRD) using a Philips PW3710 diffractometer equipped with Cu-Kα radiation. Diffraction patterns were recorded over a 2θ range

metabolic activity and, consequently, cell viability.

Statistical Analysis

All experiments were performed using at least three independent replicates, and the data are presented as mean ± standard deviation (SD). Statistical analyses were performed using Microsoft Excel 2016. Differences between experimental groups were evaluated using Student's t-test. A P-value ≤ 0.05 was considered statistically significant. Statistical significance was denoted as follows: P ≤ 0.05 (), P ≤ 0.01 (), and P < 0.001 (), where applicable.

Results

The macroscopic appearances of the PTC and PT/HC scaffolds are shown in Figure 1. Both scaffold types exhibited a well-organized, layer-by-layer architecture, with the printed filaments deposited at relatively regular intervals. The overall morphology indicated successful fabrication by 3D printing, with no apparent disruption of the general scaffold geometry following either direct incorporation of curcumin or application of the polymeric coating. The PTC scaffold exhibited a characteristic brownish-yellow coloration, consistent with the presence of curcumin within the PLA/TiO_2 matrix. In comparison, the PT/HC scaffold displayed a lighter and more uniform yellow coloration after application of the curcumin-containing HPMC coating.

FE-SEM examination of the PTC scaffold revealed relatively minor variations in filament diameter, together with several small pores and surface depressions. Despite these features, the scaffold maintained a well-defined layer-by-layer structure with satisfactory interlayer adhesion. No obvious fractures, major defects, or extensive cracks were observed between adjacent filaments.

The PT/HC scaffold exhibited a comparatively smoother surface than the PTC scaffold following application of the curcumin-containing HPMC coating. The coating covered several of the surface irregularities and shallow depressions observed in the underlying PLA/TiO_2 scaffold and produced smoother transitions between adjacent filaments.

mL of PBS and incubated at 37 ± 0.5 °C and 500 rpm using a thermoshaker. At predetermined time points, the scaffolds were removed from the incubation medium, thoroughly dried under the specified conditions, and weighed to determine their final dry weight (W_2). The percentage of weight loss, used as an indicator of scaffold degradation, was calculated according to Equation (2) [20]:

$$\text{Degradation (\%)} = [(W_1 - W_2) / W_1] \times 100$$

Cell Culture and Evaluation of Cellular Morphology

To evaluate the biological performance and cellular compatibility of the fabricated scaffolds, the samples were sterilized by exposure to ultraviolet (UV) radiation for 30 min. Each scaffold was then placed in a well of a 96-well plate and immersed in culture medium supplemented with 10% fetal bovine serum (FBS) and 1% penicillin–streptomycin. L929 fibroblasts were subsequently seeded onto each scaffold at a density of 2×10^6 cells per scaffold. The samples were maintained at 37 ± 0.5 °C in a humidified atmosphere containing 5% CO_2.

After 24 h of culture, cellular attachment, spreading, and morphology on the scaffold surfaces were examined using field-emission scanning electron microscopy (FE-SEM). For sample preparation, the cells were fixed with 3% glutaraldehyde and subsequently post-fixed with 1% osmium tetroxide for 2 h. The samples were then dehydrated through a graded ethanol series, dried, and sputter-coated with a thin layer of gold. The prepared samples were examined by FE-SEM to evaluate cellular attachment, spreading, and morphology on the scaffold surfaces.

MTT Cell Viability Assay

Cell viability was quantitatively evaluated using the MTT [3-(4,5-dimethylthiazol-2-yl)-2,5-diphenyltetrazolium bromide] assay following cell culture. At each predetermined time point, the culture medium was removed, and MTT solution was added to the wells at a final concentration of 0.5 mg/mL. Following 30 min of incubation, the resulting formazan crystals were dissolved in dimethyl sulfoxide (DMSO). The absorbance of the resulting solution was measured at 570 nm using a microplate reader. The measured optical density was used as an indicator of cellular

the apparent size or accessibility of certain pores. Nevertheless, the primary porous architecture and interfilament spaces remained discernible after coating. The morphological changes observed following coating indicate that the HPMC/curcumin layer modified the surface characteristics of the PLA/TiO_2 scaffold while preserving its overall three-dimensional architecture.

The overall three-dimensional architecture of the scaffold remained clearly identifiable after coating, and no substantial deformation or structural collapse was observed. The coating appeared to form a continuous layer over substantial portions of the filament surfaces.

Closer examination of the PT/HC scaffold showed partial coverage of some surface openings by the HPMC-based coating, resulting in a reduction in

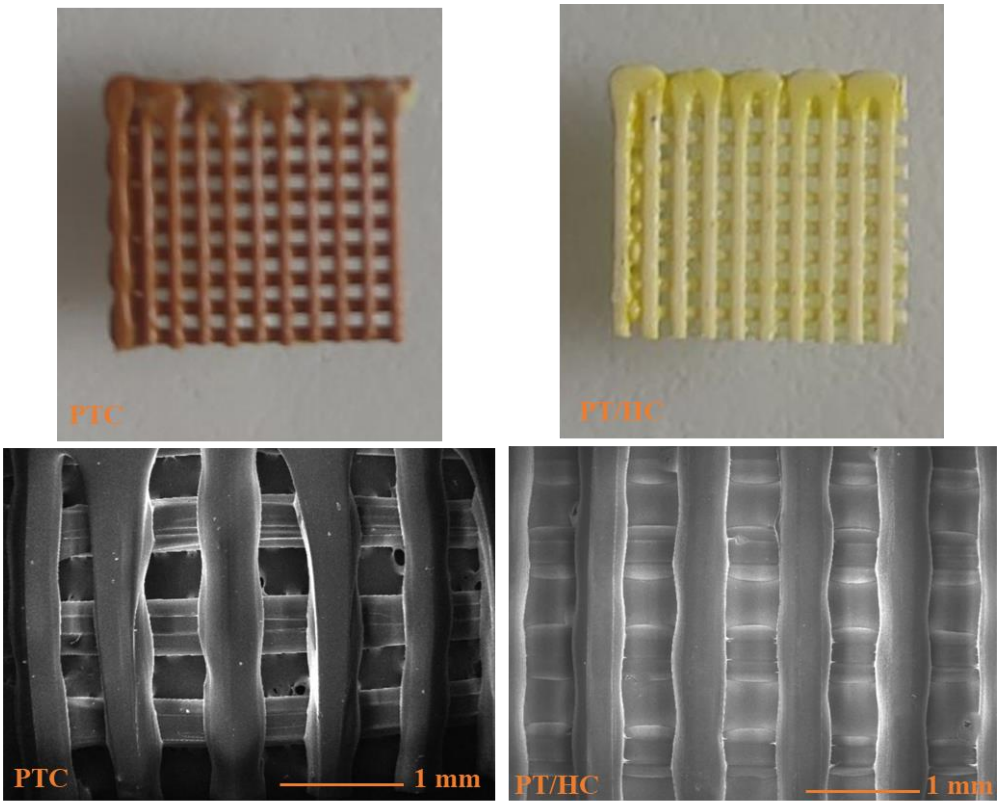

Figure 2: FTIR spectra of the PT, PTC, and PT/HC scaffolds

consistent with the presence of TiO_2 in the composite matrix. Broad absorption bands in the 3400–3600 cm^{-1} region were also observed and were assigned to O–H stretching vibrations, which may be associated with hydroxyl groups and/or adsorbed moisture.

The spectra of the curcumin-containing scaffolds exhibited additional absorption features corresponding to characteristic functional groups of curcumin. These included an O–H stretching band at approximately 3506 cm^{-1}, a C–O–C-related band near 1020 cm^{-1}, and absorption bands in the approximately 1508 and 1626 cm^{-1} regions associated with characteristic curcumin vibrational modes. These spectral features were observed in both the PTC and PT/HC scaffolds,

The FTIR spectra of the PT, PTC, and PT/HC scaffolds are presented in Figure 2. The spectrum of the PT scaffold exhibited a prominent absorption band at approximately 1750 cm^{-1}, corresponding to the stretching vibration of the ester carbonyl (C=O) group characteristic of PLA. Absorption bands associated with the asymmetric and symmetric stretching vibrations of C–H groups were observed in the 2881–2990 cm^{-1} region. In addition, a band attributed to the bending vibration of the CH_3 group was detected at approximately 1452 cm^{-1} in all three scaffold groups.

In the region below 800 cm^{-1}, absorption bands attributable to Ti–O and Ti–O–Ti vibrations were observed in the spectra of all three scaffold types,

approximately 1750 cm^{-1} remained clearly detectable in the PT/HC spectrum, indicating that the surface-coating process did not obscure the principal chemical signature of the underlying PLA matrix.

Overall, the FTIR spectra demonstrated the characteristic spectral features of PLA, TiO_2, curcumin, and HPMC in the corresponding scaffold formulations, with no major changes in the principal absorption bands of the constituent materials following scaffold fabrication and curcumin incorporation.

with comparatively greater absorption intensities evident in the PTC spectrum.

The PT/HC spectrum also displayed an absorption band associated with C–H stretching at approximately 2932 cm^{-1} and an O–H stretching band near 3430 cm^{-1}. An additional band at approximately 1380 cm^{-1} was assigned to O–H bending vibrations. Furthermore, increased absorption intensity was observed in the 1050–1150 cm^{-1} region in the PT/HC spectrum, consistent with the contribution of the HPMC coating. The characteristic PLA carbonyl band at

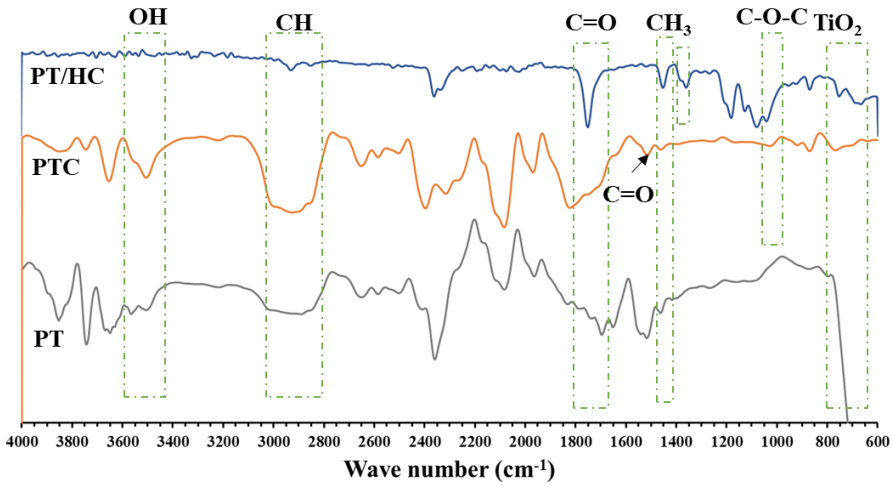

Figure 2: FTIR spectra of the PT, PTC, and PT/HC scaffolds

percentage of mass loss reached 14.03 ± 0.0% for PTC and 14.27 ± 0.0% for PT/HC.

At the evaluated time points, PT/HC generally exhibited slightly greater mass loss than PTC. The degradation profile of PT/HC showed a distinct two-stage pattern, with a relatively more pronounced increase in mass loss during the initial phase followed by a slower rate of mass loss during the subsequent period. In contrast, PTC exhibited a more gradual and relatively uniform increase in mass loss throughout the 28-day observation period. The differences in degradation profiles indicate that the two curcumin-loading strategies influenced the mass-loss behavior of the scaffolds under the experimental conditions.

The swelling ratios of the scaffolds after 24 h of immersion in phosphate-buffered saline (PBS) at 37 °C are presented in Figure 3A. The PTC scaffold exhibited a swelling ratio of 161 ± 7.6%, whereas the PT/HC scaffold exhibited a slightly higher swelling ratio of 166 ± 0.5%. Thus, PT/HC demonstrated a greater water-uptake capacity than PTC under the experimental conditions. However, the difference between the two scaffold groups was relatively small.

The degradation profiles of the scaffolds over 28 days are presented in Figure 3B. Both PTC and PT/HC exhibited progressive mass loss throughout the incubation period. After 28 days, the

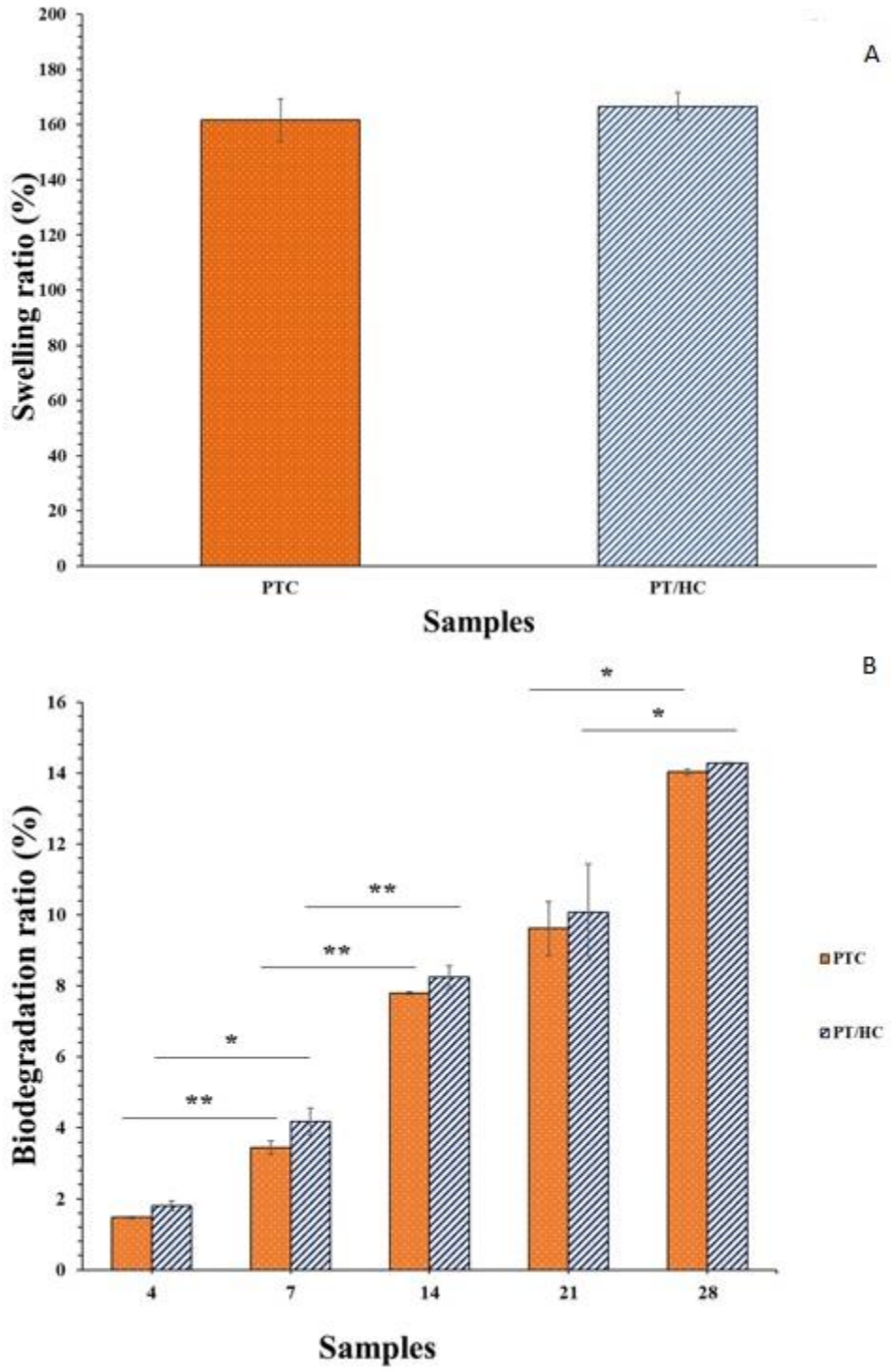

Figure 3: Swelling (A) and degradation (B) of the PTC and PT/HC scaffolds in phosphate-buffered saline

FE-SEM images showed that cells successfully attached to both the PTC and PT/HC scaffolds and were distributed across the scaffold surfaces. Visually, the PTC scaffold exhibited a greater number of attached cells and a more uniform

The cellular biocompatibility of the fabricated scaffolds was evaluated using field-emission scanning electron microscopy (FE-SEM) and the MTT assay, with the corresponding results presented in Figure 4A–C.

viability increased from 87.66 ± 2.14% on day 1 to 88.49 ± 3.25% on day 7.

At all evaluated time points, the PTC scaffold exhibited higher cell viability than the PT/HC scaffold. Overall, both scaffold formulations maintained relatively high cell viability throughout the 7-day culture period, with PTC showing the more favorable cellular response under the experimental conditions.

cellular distribution than the PT/HC scaffold. The cells displayed an adherent morphology and appeared to spread across the scaffold surfaces.

Quantitative evaluation using the MTT assay showed that cell viability remained above 85% on both scaffold types throughout the 7-day culture period. For the PTC scaffold, cell viability increased from 90.7 ± 0.26% on day 1 to 93.6 ± 1.6% on day 7. On the PT/HC scaffold, cell

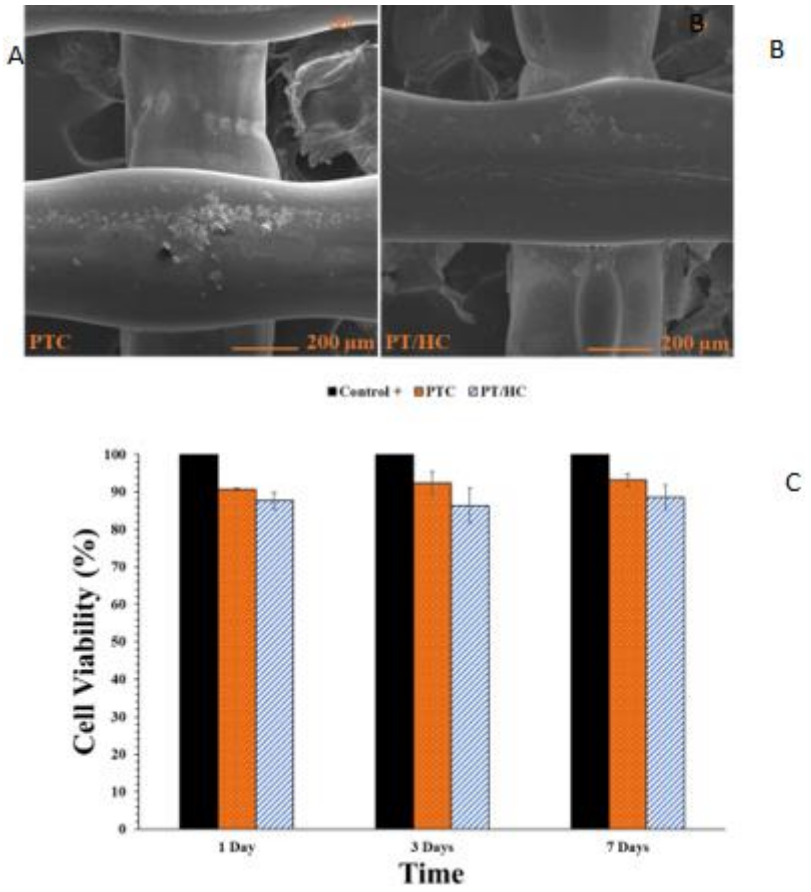

Figure 4: FE-SEM images of cells cultured on the PTC (A) and PT/HC (B) scaffolds, and cell viability measured over 7 days of culture on the PTC and PT/HC scaffolds (C)

The main novelty of this study lies in the direct comparison of two distinct curcumin-loading strategies within the same PLA/TiO_2 scaffold platform. Unlike previous studies that have primarily investigated curcumin-containing scaffolds as individual formulations, the present study directly compares curcumin incorporation into the PLA/TiO_2 matrix before 3D printing with post-printing surface loading of curcumin through an HPMC-based coating under comparable experimental conditions. This comparative design

Discussion

Curcumin, one of the principal bioactive constituents of the rhizome of *Curcuma longa* L. (turmeric), has attracted considerable interest as a plant-derived compound for the development of bioactive materials for tissue engineering because of its antioxidant and anti-inflammatory properties and its reported potential to support bone regeneration.

O/C–O–C regions, further supported the presence of the polymeric coating [26].

The slightly higher swelling ratio observed for PT/HC compared with PTC is consistent with the hydrophilic nature of HPMC. The abundant hydroxyl groups of HPMC can interact with water molecules and promote water uptake and retention within the polymeric coating [27–29]. Increased water uptake may enhance surface hydration and facilitate penetration of the aqueous medium into the coating. Nevertheless, the relatively small difference in swelling between the two formulations suggests that incorporation of the HPMC/curcumin coating did not substantially alter the overall water-uptake behavior of the scaffolds under the conditions tested. Maintaining controlled swelling is relevant to bone tissue-engineering applications because excessive swelling could alter scaffold dimensions and pore architecture, whereas an appropriate degree of hydration may support cellular interactions with the biomaterial.

The degradation profiles also revealed differences between the two curcumin-loading strategies. PT/HC exhibited slightly greater mass loss than PTC over the 28-day incubation period, particularly during the earlier phase of the experiment. This behavior may be related to the greater water accessibility of the HPMC-based surface layer and its susceptibility to dissolution, erosion, or structural changes during aqueous incubation [30,31]. Because the HPMC-containing layer is directly exposed to the surrounding medium, its contribution to the early mass loss of PT/HC may be greater than that of the underlying PLA/TiO_2 matrix. As the coating is progressively removed or altered, the subsequent degradation behavior would be expected to increasingly reflect the properties of the underlying PLA/TiO_2 scaffold. PLA degradation generally occurs through hydrolytic cleavage of ester bonds following water penetration into the polymer matrix, with degradation kinetics influenced by factors such as crystallinity, molecular weight, morphology, and the accessibility of the polymer chains to water [32]. Thus, the distinct degradation profile of PT/HC may reflect the presence of an additional surface layer with different water-interaction and degradation characteristics from those of the PLA/TiO_2 matrix.

enables the influence of the loading strategy on scaffold physicochemical properties, degradation behavior, and cellular response to be evaluated and provides practical insight into the selection of an appropriate approach for developing plant-bioactive-containing scaffolds for bone tissue engineering.

However, the biological performance of curcumin in biomaterial systems depends not only on its intrinsic biological properties but also on its incorporation strategy, physicochemical environment, stability, and release characteristics. In the present study, two approaches for incorporating turmeric-derived curcumin into PLA/TiO_2 scaffolds were comparatively evaluated: direct incorporation into the scaffold matrix (PTC) and post-printing incorporation within an HPMC-based coating (PT/HC). The two formulations were subsequently compared in terms of their chemical characteristics, swelling behavior, degradation profile, and cellular response.

The FTIR findings indicated that the principal chemical characteristics of the PLA/TiO_2 matrix were retained following curcumin incorporation and application of the HPMC-based coating. The prominent PLA carbonyl band at approximately 1750 cm^{-1} and the C–H stretching bands in the 2881–2990 cm^{-1} region were consistent with characteristic spectral features of PLA [21,22]. Absorption bands below 800 cm^{-1} attributable to Ti–O and Ti–O–Ti vibrations were also observed, consistent with the presence of TiO_2 in the composite scaffolds [23]. In addition, characteristic absorption features associated with curcumin, including bands related to O–H, C–O–C, and C=O-containing functional groups, were detected in both PTC and PT/HC [24,25]. These findings provide spectral evidence supporting the incorporation of curcumin into both scaffold formulations. Changes in the intensity of selected O–H, C=O, and C–O-related bands in PTC may reflect intermolecular interactions, including possible hydrogen bonding, between curcumin and the polymeric matrix. However, because no distinct new absorption bands were observed, the FTIR results do not provide evidence for the formation of new covalent chemical bonds among the principal scaffold components. In PT/HC, additional spectral features associated with HPMC, particularly in the O–H, C–H, and C–

be advantageous when modification of surface hydration or more accessible exposure of the plant-derived bioactive compound is desired. However, the optimal loading strategy ultimately depends on the intended application and the desired balance among curcumin availability, scaffold stability, degradation behavior, and cellular response.

Overall, the present findings support the potential of turmeric-derived curcumin as a plant-based bioactive component of three-dimensionally printed PLA/TiO_2 scaffolds for bone tissue-engineering applications. The incorporation of a bioactive constituent derived from *C. longa* into a structurally defined polymeric scaffold provides a promising approach for integrating the biological properties of a medicinal plant-derived compound with the architectural and functional advantages of 3D-printed biomaterials. Further studies incorporating direct curcumin-release measurements, longer-term degradation analysis, osteogenic differentiation assays, and in vivo evaluation are warranted to clarify the mechanisms underlying the observed cellular responses and to determine the regenerative potential of these curcumin-containing scaffolds.

Despite the promising findings, this study has several limitations, including the lack of direct evaluation of curcumin release kinetics, osteogenic differentiation, and in vivo performance. Future studies should investigate curcumin release and availability, osteogenic differentiation markers, and scaffold performance in appropriate animal models to better establish the bone-regenerative potential and translational applicability of these curcumin-loaded scaffolds.

Future studies should include appropriate and well-defined control groups, such as PLA, PLA/TiO_2, and PLA/TiO_2/curcumin scaffolds, to distinguish the independent contributions of PLA, TiO_2, and curcumin and thereby enable a more accurate interpretation of their respective effects on the biological responses of the scaffolds.

Conclusion

This study demonstrated that turmeric-derived curcumin can be incorporated into 3D-printed PLA/TiO_2 scaffolds using either direct matrix incorporation or post-printing HPMC-based

The cellular findings demonstrated favorable cellular responses to both scaffold formulations during the 7-day culture period. FE-SEM observations showed cellular attachment and spreading on both PTC and PT/HC, while the PTC scaffold exhibited a visually greater number of attached cells and a more homogeneous cellular distribution. Consistent with these observations, the MTT assay showed that cell viability remained above 85% throughout the culture period for both formulations. However, PTC exhibited higher cell viability than PT/HC at the evaluated time points. These findings suggest that the strategy used to incorporate curcumin may influence the biological response of the resulting scaffold.

The comparatively favorable cellular response observed for PTC may be related to differences in the physicochemical environment surrounding curcumin in the two formulations. Direct incorporation within the PLA/TiO_2 matrix may restrict the immediate accessibility of curcumin to the aqueous culture medium, whereas the HPMC-based surface coating is more hydrophilic and therefore more readily hydrated. Such differences could influence the availability of curcumin at the scaffold–cell interface. However, because curcumin-release kinetics were not directly measured in the present study, the possibility of differences in release rate should be regarded as a plausible explanation rather than a demonstrated mechanism. Similarly, although curcumin possesses well-established antioxidant and anti-inflammatory properties, its effects on cellular behavior may depend on concentration, exposure duration, cell type, and the physicochemical characteristics of the delivery system. Therefore, the lower viability observed for PT/HC should not be attributed specifically to a higher initial curcumin concentration without direct release and concentration measurements.

The findings collectively indicate that both curcumin-loading strategies can be used to produce PLA/TiO_2 scaffolds with favorable cellular responses. Nevertheless, direct incorporation of curcumin into the PLA/TiO_2 matrix resulted in a comparatively more favorable cellular response than post-printing loading through the HPMC-based coating. In contrast, the HPMC coating increased the hydrophilic character of the scaffold and was associated with a distinct early mass-loss profile. These characteristics may

2024;25(23):12766. doi:10.3390/ijms252312766.
8. Ivanova N, Ivanov S, Peev S, Dikova T. Types of bone substitutes and their application in regenerative medicine: a systematic review. J Funct Biomater. 2025;16(9):341. doi:10.3390/jfb16090341.
9. Ashammakhi N, Ahadian S, Xu C, Montazerian H, Ko H, Nasiri R, et al. Bioinks and bioprinting technologies to make heterogeneous and biomimetic tissue constructs. Mater Today Bio. 2019;1:100008. doi:10.1016/j.mtbio.2019.100008.
10. Sahranavard M, Zamanian A, Ghorbani F, Shahrezaee MH. A critical review on three-dimensional-printed chitosan hydrogels for development of tissue engineering. Bioprinting. 2020;17:e00063. doi:10.1016/j.bprint.2019.e00063.
11. Gebeshuber IC, Khawas S, Sharma R, Sharma N. Bioprinted scaffolds for biomimetic applications: a state-of-the-art technology. Biomimetics. 2025;10(9):595. doi:10.3390/biomimetics10090595.
12. Sahranavard M, Sarkari S, Safavi S, Ghorbani F. Three-dimensional bio-printing of decellularized extracellular matrix-based bio-inks for cartilage regeneration: a systematic review. Biomater Transl. 2022;3:2. doi:10.12336/biomatertransl.2022.02.004.
13. Yücer S, Sarac B, Ciftci F. Bioprinting revolution: innovative design of 3D bioactive scaffolds for living organs and transdermal tissues. Bioeng Transl Med. 2025;10:e70080. doi:10.1002/btm2.70080.
14. Wang W, Zhang B, Li M, Li J, Zhang C, Han Y, et al. 3D printing of PLA/n-HA composite scaffolds with customized mechanical properties and biological functions for bone tissue engineering. Compos Part B Eng. 2021;224:109192. doi:10.1016/j.compositesb.2021.109192.
15. Moradi R, Vaseghi M, Sohrabian M, Vanaei HR. Optimized bioactive glass/PLA nanocomposites for bone tissue engineering: balancing mechanical strength and biodegradability. Int J Polym Mater Polym Biomater. 2025;74:1596-1609. doi:10.1080/00914037.2025.2477164.

coating while preserving the overall scaffold architecture and cellular compatibility. The major novelty of the study was the direct comparison of these two curcumin-loading strategies within the same PLA/TiO_2 scaffold platform. Direct incorporation of curcumin (PTC) resulted in a more favorable cellular response, with higher cell viability and greater cellular attachment than the post-printing HPMC/curcumin coating approach. These findings highlight the potential of combining a medicinal-plant-derived bioactive compound with 3D-printed biomaterials to develop multifunctional scaffolds for bone tissue engineering. Further studies should evaluate curcumin-release kinetics, osteogenic differentiation, and in vivo bone regeneration to establish the regenerative and translational potential of these scaffolds.

References

1. Šromová V, Sobola D, Kaspar P. A brief review of bone cell function and importance. Cells. 2023;12(21):2576. doi:10.3390/cells12212576.
2. Wawrzyniak A, Balawender K. Structural and metabolic changes in bone. Animals (Basel). 2022;12(15):1946. doi:10.3390/ani12151946.
3. Rahmani A, Weichelt U, Jahn D, Otto E, Kienzle A, Angelov S, et al. Beyond the initial impact: a systematic review of post-traumatic bone loss and its mechanisms. Osteoporos Int. 2026;37:15-39. doi:10.1007/s00198-025-07716-6.
4. Buettmann EG, Goldscheitter GM, Hoppock GA, Friedman MA, Suva LJ, Donahue HJ. Similarities between disuse and age-induced bone loss. J Bone Miner Res. 2020;37:1417-1434. doi:10.1002/jbmr.4643.
5. Zioupos P. Ageing human bone: factors affecting its biomechanical properties and the role of collagen. J Biomater Appl. 2001;15:187-229. doi:10.1106/5JUJ-TFJ3-JVVA-3RJ0.
6. De Pace R, Molinari S, Mazzoni E, Perale G. Bone regeneration: a review of current treatment strategies. J Clin Med. 2025;14(6):1838. doi:10.3390/jcm14061838.
7. Łuczak JW, Palusińska M, Matak D, Pietrzak D, Nakielski P, Lewicki S, et al. The future of bone repair: emerging technologies and biomaterials in bone regeneration. Int J Mol Sci.

processing: highly enhanced bioavailability, fluorescence, and anti-cancer efficacy. RSC Adv. 2014;4:60334-60341. doi:10.1039/C4RA07300B.
25. Mohamed Ibrahim R, El Zahraa Ali Abd Elaal F, Zaki S. Effect of curcumin and nano-curcumin on reduce aluminum toxicity in rats. Int J Food Sci Biotechnol. 2019;4:64. doi:10.11648/j.ijfsb.20190403.12.
26. Tomar P, Kumar R, Lakhani R, Srivastava A, Chhibber VK. Improvement in hygroscopic property of macro-defect free cement modified with hypromellose/potassium methyl siliconate copolymer and pulverized fly ash. J Therm Anal Calorim. 2022;147:12417-12430. doi:10.1007/s10973-022-11447-9.
27. Dahlan A, Kamadjaja MJK, Subagyo SY, Talitha P. Evaluation of swelling ability of scaffold combination of chitosan and hydroxyapatite. Indones J Prosthodont. 2022;3:17-22. doi:10.46934/ijp.v3i1.134.
28. Farshi Azhar F, Olad A, Salehi R. Fabrication and characterization of chitosan-gelatin/nanohydroxyapatite-polyaniline composite with potential application in tissue engineering scaffolds. Des Monomers Polym. 2014;17:654-667. doi:10.1080/15685551.2014.907621.
29. Vlad RA, Pintea A, Pintea C, Rédai EM, Antonoaea P, Bîrsan M, et al. Hydroxypropyl methylcellulose—a key excipient in pharmaceutical drug delivery systems. Pharmaceutics. 2025;17(6):784. doi:10.3390/pharmaceutics17060784.
30. Joshi SR, Pendyala GS, Shah P, Mopagar VP, Padmawar N, Padubidri M. Scaffolds—the ground for regeneration: a narrative review. J Int Soc Prev Community Dent. 2020;10:692-699. doi:10.4103/jispcd.JISPCD_198_20.
31. Deshmukh K, Ahamed MB, Deshmukh RR, Pasha SKK, Bhagat PR, Chidambaram K. Biopolymer composites with high dielectric performance: interface engineering. In: Biopolymer composites in electronics. Elsevier; 2017. p.27-128. doi:10.1016/B978-0-12-809261-3.00003-6.
32. Feng P, Jia J, Liu M, Peng S, Zhao Z, Shuai C. Degradation mechanisms and
16. Shafaghi R, Rodriguez O, Phull S, Schemitsch EH, Zalzal P, Waldman SD, et al. Effect of TiO2 doping on degradation rate, microstructure and strength of borate bioactive glass scaffolds. Mater Sci Eng C Mater Biol Appl. 2020;107:110351. doi:10.1016/j.msec.2019.110351.
17. Xie Q, Wang T, He L, Liang H, Sun J, Huang X, et al. Biological and structural properties of curcumin-loaded graphene oxide incorporated collagen as composite scaffold for bone regeneration. Front Bioeng Biotechnol. 2024;12:1505102. doi:10.3389/fbioe.2024.1505102.
18. Astaneh ME, Noori F, Fereydouni N. Curcumin-loaded scaffolds in bone regeneration. Heliyon. 2024;10:e32566. doi:10.1016/j.heliyon.2024.e32566.
19. Ghorbani F, Zamanian A, Sahranavard M. Mussel-inspired polydopamine-mediated surface modification of freeze-cast poly(ε-caprolactone) scaffolds for bone tissue engineering applications. Biomed Tech (Berl). 2020;65:273-287. doi:10.1515/bmt-2019-0061.
20. Sahranavard M, Zamanian A, Ghader AB, Shahrezaee M. Optimization of gellan gum-based bioink printability for precision 3D bioprinting in tissue engineering. Int J Biol Macromol. 2025;320:145800. doi:10.1016/j.ijbiomac.2025.145800.
21. Cuevas-Carballo ZB, Duarte-Aranda S, Canché-Escamilla G. Properties and biodegradation of thermoplastic starch obtained from grafted starches with poly(lactic acid). J Polym Environ. 2019;27:2607-2617. doi:10.1007/s10924-019-01540-w.
22. Chieng B, Ibrahim N, Yunus W, Hussein M. Poly(lactic acid)/poly(ethylene glycol) polymer nanocomposites: effects of graphene nanoplatelets. Polymers (Basel). 2013;6:93-104. doi:10.3390/polym6010093.
23. Chougala LS, Yatnatti MS, Linganagoudar RK, Kamble RR, Kadadevarmath JS. A simple approach on synthesis of TiO2 nanoparticles and its application in dye sensitized solar cells. J Nano-Electron Phys. 2017;9(4):04005-1-04005-6. doi:10.21272/jnep.9(4).04005.
24. Singh PK, Wani K, Kaul-Ghanekar R, Prabhune A, Ogale S. From micron to nano-curcumin by sophorolipid co-

Mater Des. 2021;210:110066. doi:10.1016/j.matdes.2021.110066.

acceleration strategies of poly(lactic acid) scaffold for bone regeneration.